

**Nonyrast states in the odd-odd  $N=Z$  nucleus  $^{62}\text{Ga}$** D. Rudolph, C. Andreoiu,\* J. Ekman, C. Fahlander, and M. N. Mineva  
*Department of Physics, Lund University, S-22100 Lund, Sweden*S. M. Lenzi, E. Farnea, C. Rossi-Alvarez, and C. A. Ur  
*Dipartimento di Fisica dell'Università and INFN, Sezione di Padova, I-35141 Padova, Italy*M. Axiotis, G. de Angelis, A. Gadea, Th. Kröll,† N. Mărginean, and T. Martinez  
*Instituto Nazionale di Fisica Nucleare, Laboratori Nazionali di Legnaro, I-35020 Legnaro, Italy*

F. Nowacki

*Laboratoire de Physique Théorique, F-67084 Strasbourg Cedex, France*

(Received 3 March 2003; revised manuscript received 12 December 2003; published 4 March 2004)

Low-lying excited states in the odd-odd  $N=Z$  nucleus  $^{62}\text{Ga}$  have been investigated following the heavy-ion fusion-evaporation reaction  $^{40}\text{Ca}(^{24}\text{Mg}, pn)^{62}\text{Ga}$  near the Coulomb barrier. Special emphasis is devoted to the search for nonyrast states. The extended decay scheme of  $^{62}\text{Ga}$  is compared to spherical shell-model calculations employing the  $pf_{5/2g_{9/2}}$  valence space.

DOI: 10.1103/PhysRevC.69.034309

PACS number(s): 21.60.Cs, 23.20.Lv, 21.10.Sf, 27.50.+e

**I. INTRODUCTION**

The advent of the latest generation of large  $\gamma$ -ray spectrometers and their coupling to powerful ancillary devices initiated comprehensive experimental in-beam studies of medium mass,  $A \sim 50$ – $90$ , self-conjugate  $N=Z$  nuclei. Along the  $N=Z$  line neutrons and protons fill identical orbitals and their wave functions have large spatial overlap, which leads to a reinforcement of shell structures and effects arising from isospin  $T=0$  and  $T=1$  neutron-proton pairing correlations. Another facet of  $N \sim Z$  nuclei is the test of isospin symmetry of the nuclear forces by studying, for example,  $T_z = \pm 1/2$  mirror nuclei. A recent summary of both in-beam and decay work as well as theoretical developments regarding  $N=Z$  nuclei is Ref. [1].

Odd-odd  $N=Z$  nuclei are special as  $T=0$  and  $T=1$  states compete at low excitation energies. Having good knowledge on isospin, spin, parities, energies, and electromagnetic decay properties of low-lying states in these nuclei allows for detailed investigations of different pairing modes [2,3] or the amount of isospin mixing [4]. Up to mass  $A=58$  such studies are feasible in the  $fp$  shell with present techniques and spectrometers, not least because information gained from heavy-ion fusion evaporation reactions [2,3,5,6], which favor high-spin states along the yrast line, can be combined with results from low-spin studies using, for example,  $(p, n\gamma)$  reactions [7–10]. The latter reaction type can probe nonyrast states as well. Beyond  $A=58$  light-ion induced reactions are no longer possible because of the lack of suitable stable target materials. Therefore, it is increasingly difficult to identify the

$T=1$  states as they typically move away quickly from the yrast line with increasing spin. They are thus difficult to access via heavy-ion fusion evaporation reactions. Nevertheless, candidates for the  $T=1$   $2^+$  and  $4^+$  isobaric analog states exist in  $^{74}\text{Rb}$  [11], and they have recently been established in  $^{70}\text{Br}$  [12,13]. The candidates proposed in Ref. [12] for the  $6^+$  and  $8^+$  isobaric analog states have been disputed in Ref. [13]. This paper presents a nonyrast study of  $^{62}\text{Ga}$  to search for the even-spin  $T=1$  isobaric analog states, since none of them is known in  $^{62}\text{Ga}$  from the previous in-beam work [14,15].

**II. EXPERIMENT**

The experiment was performed at the Tandem XTU accelerator facility at Legnaro National Laboratory, Italy. The fusion-evaporation reaction  $^{24}\text{Mg} + ^{40}\text{Ca}$  at 60 MeV beam energy was used to populate excited states in  $N \sim Z$  nuclei in the mass  $A \sim 60$  region. The beam energy was chosen close to the Coulomb barrier in order not to open too many reaction channels and to increase the probability of feeding nonyrast structures in the various residual nuclei. In the  $0.5 \text{ mg/cm}^2$  thin, enriched  $^{40}\text{Ca}$  target layer the beam energy decreased to some 55 MeV, for which no significant fusion cross section is predicted anymore. The target layer was backed by a  $7 \text{ mg/cm}^2$  tantalum foil to stop the recoiling nuclei. The front side of the target was covered with a thin flash of gold to prevent oxidation. Nevertheless, small but noticeable amounts of  $^{12}\text{C}$ ,  $^{16}\text{O}$ ,  $^{44}\text{Ca}$ , and  $^{nat}\text{Mg}$  were identified as target contaminants [17].

The  $\gamma$  rays produced in the reactions were detected with the GASP Ge-detector array [18] including 40 Compton-suppressed high-purity Ge-detector elements and 74 out of the standard 80 BGO elements. At the most forward angles the NeutronRing array replaced six BGO elements to allow for the detection of evaporated neutrons. The system was coupled to the  $4\pi$  charged-particle detector ISIS [19] con-

\*Present address: Department of Physics, University of Guelph, Guelph, Ontario, Canada N1G 2W1.

†Present address: Physik-Department, Technische Universität München, D-85748 Garching, Germany.

TABLE I. Experimental relative fusion cross sections  $\sigma_{rel}$  of the reaction  $^{24}\text{Mg}+^{40}\text{Ca}$  at 60 MeV initial beam energy. The predicted total fusion cross section averaged over the target thickness is 110 mb.

Nuclide	Channel	$\sigma_{rel}$ (%)
$^{62}\text{Ga}$	$1p1n$	0.25(2)
$^{62}\text{Zn}$	$2p$	6.7(5)
$^{61}\text{Zn}$	$2p1n$	8.4(6)
$^{61}\text{Cu}$	$3p$	57(4)
$^{60}\text{Cu}$	$3p1n$	0.22(4)
$^{59}\text{Cu}$	$1\alpha1p$	1.8(3)
$^{58}\text{Cu}$	$1\alpha1p1n$	0.17(3)
$^{60}\text{Ni}$	$4p$	1.8(2)
$^{58}\text{Ni}$	$1\alpha2p$	20(3)
$^{56}\text{Ni}$	$2\alpha$	0.07(2)
$^{57}\text{Co}$	$1\alpha3p$	<0.1
$^{55}\text{Co}$	$2\alpha1p$	0.02(1)

sisting of 40  $\Delta E-E$  Si telescopes to detect evaporated charged particles. The coincident detection of evaporated particles and  $\gamma$  radiation thus allows to discriminate  $\gamma$  rays originating from different reaction products. The event trigger required either one Ge detector, one BGO detector, and one neutron detector or two Ge detectors and one BGO detector firing. At the end of the experiment, the Ge detectors were energy and efficiency calibrated with  $^{56}\text{Co}$ ,  $^{133}\text{Ba}$ , and  $^{152}\text{Eu}$  sources.

### III. RESULTS

Table I shows the experimental relative cross sections for the reaction  $^{24}\text{Mg}+^{40}\text{Ca}$  at beam energies ranging from ini-

tially 60 MeV down to 55 MeV. They are estimated from the efficiency corrected yields of known ground-state and band-head transitions in various spectra with different conditions on evaporated charged particles or neutrons.

$^{62}\text{Ga}$  residues are formed after the evaporation of one proton and one neutron from the compound nucleus  $^{64}\text{Ge}$ . They are produced in about 0.3% of the reactions. The result of the analysis of particle-gated  $\gamma\gamma$  and  $\gamma\gamma\gamma$  coincidences as well as  $\gamma\gamma$  angular distributions and correlations is comprised in the excitation scheme of  $^{62}\text{Ga}$  displayed on the left hand side of Fig. 1 and the corresponding numeric details in Table II. The RADWARE analysis software [20] and the spectrum analysis code TV [21] were employed to derive the results.

The level scheme shown in Fig. 1 is consistent with the one proposed by Vincent *et al.* [14], who reported the 571-246-376-1241-2355-946-1107 keV yrast cascade and the 622 and 1180 keV transitions populating the  $3^+$  and  $5^+$  states, respectively. In an independent high-spin study of  $^{62}\text{Ga}$  [15], the 1488-867 keV bypass of the 2355 keV transition has been observed together with the extension of the odd-spin yrast sequence up to spin  $I=17$  via two additional stretched quadrupole transitions at 1747 and 1387 keV. The other transitions on the right hand side of the level scheme in Fig. 1 are inferred from the present work. In the following, their coincidence relationships are going to be discussed in more detail based on the  $\gamma$ -ray spectra displayed in Figs. 2 and 3.

Figure 2 provides a total of four  $\gamma$ -ray spectra, which originate from a  $\gamma\gamma\gamma$  analysis, i.e., they are measured in coincidence with certain combinations of two  $\gamma$ -ray transitions. Panel (b) may be regarded as a  $^{62}\text{Ga}$  reference spectrum as it relates to the sum the three spectra in coincidence with any combination of the three intense, low-lying 246, 376, and 571 keV transitions. The inset shows the high-energy fraction of the spectrum highlighting the known 2355 keV line and a new, tentative transition at 2603 keV. Weak new lines at 1363 and 1424 keV are also present in

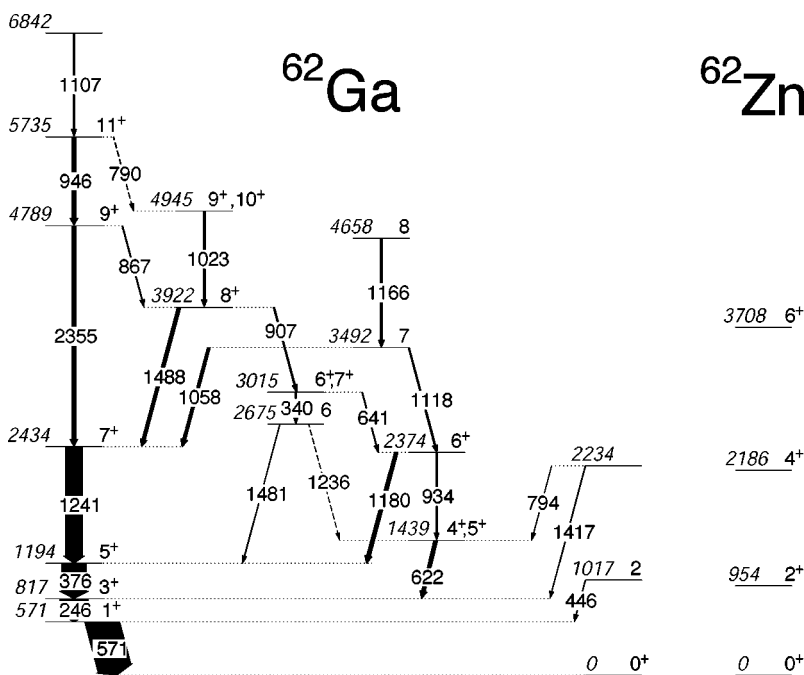


FIG. 1. Proposed partial level scheme of  $^{62}\text{Ga}$ . The energy labels are given in keV. The widths of the arrows are proportional to the relative intensities of the  $\gamma$  rays. Tentative transitions are dashed. On the right hand side the yrast  $0^+$ ,  $2^+$ ,  $4^+$ , and  $6^+$  states of  $^{62}\text{Zn}$  [16] are shown.

TABLE II. The energies of excited states in  $^{62}\text{Ga}$ , the transition energies and relative intensities of the  $\gamma$  rays placed in the level scheme, angular correlation and distribution ratios, and the spins and parties of the initial and final states of the  $\gamma$  rays.

$E_x$ (keV)	$E_\gamma$ (keV)	$I_{rel}$ (%)	$R_{DCO}(35^\circ - 81^\circ)^a$	$R_{35-90}$	Multipole assignment	$I_i^\pi$ ( $\hbar$ )	$I_f^\pi$ ( $\hbar$ )
571.2(1)	571.2(1)	120(4)	0.59(3)	0.77(3)	$M1$	$1^+$	$0^{+b}$
817.2(1)	246.0(1)	100(3)	0.92(6)	1.30(3)	$E2$	$3^+$	$1^+$
1016.7(3)	445.5(3)	1.7(2)		0.58(9)	$\Delta I=1$	2	$1^+$
1193.5(2)	376.3(1)	89(3)	1.05(6)	1.35(5)	$E2$	$5^+$	$3^+$
1439.4(2)	622.3(1)	13.0(5)	1.06(16)	1.37(10)	$E2/M1, E2$	$4^+, 5^+$	$3^+$
2234.0(5)	794.4(5)	1.7(6)		1.57(64)			$4^+, 5^+$
	1417(1)	2.6(7)		0.77(23)			$3^+$
2373.6(3)	934.2(4)	3.8(4)		1.22(28)		$6^{+c}$	$4^+, 5^+$
	1180.1(3)	12.7(5)	0.93(12)	0.97(6)	$E2/M1$	$6^+$	$5^+$
2434.3(2)	1240.7(2)	62(2)	0.99(7)	1.26(5)	$E2$	$7^+$	$5^+$
2674.5(3)	1236(1)	1(1)				6	$4^+, 5^+$
	1481(1)	1.8(3)		0.62(11)	$\Delta I=1$	6	$5^+$
3014.8(3)	340.4(2)	3.2(7)		1.70(58)		$6^+, 7^+$	6
	641.2(2)	2.7(3)	0.89(24)	1.26(18)	$\Delta I=0, E2/M1$	$6^+, 7^+$	$6^+$
3491.8(3)	1057.6(2)	11.4(5)	0.95(13)	1.32(7)	$\Delta I=0$	$7^c$	$7^+$
	1118.2(2)	5.3(5)	0.70(16)	0.77(8)	$\Delta I=1$	7	$6^+$
3922.0(3)	907.3(3)	5.5(6)	1.09(22)	0.87(9)	$E2/M1, E2$	$8^+$	$6^+, 7^+$
	1487.7(3)	12.3(6)	0.36(6)	0.61(4)	$E2/M1$	$8^+$	$7^+$
4657.8(4)	1166.0(3)	7.6(4)	1.17(19)	1.05(9)	$E2/M1$	$8^c$	7
4789.1(3)	867.1(2)	3.6(3)	0.41(10)	0.55(8)	$E2/M1$	$9^+$	$8^+$
	2354.8(5)	13.6(10)	1.21(17)	1.37(10)	$E2$	$9^+$	$7^+$
4945.2(4)	1023.1(2)	8.0(5)	0.91(16)	1.12(8)	$E2/M1, E2$	$9^+, 10^+$	$8^+$
5735.0(4)	789.5(6)	1.1(6)				$11^+$	$9^+, 10^+$
	945.9(2)	16.0(6)	1.09(11)	1.38(8)	$E2$	$11^+$	$9^+$
6842.3(5)	1107.3(3)	5.9(7)					$11^+$

<sup>a</sup>The 246 and 376 keV  $E2$  transitions were used for gating. See text for details.

<sup>b</sup>The 571 keV transition is assumed to be the ground-state transition. Subsequent spin and parity assignments are based on this assumption.

<sup>c</sup>Spin and parity assignment also based on yrast and  $\gamma$ -ray intensity arguments. See text for details.

Fig. 2(b). These three lines may decay from a new level at 3797 keV into the known states at 1194, 2374, and 2434 keV, respectively. However, due to insufficient coincidence statistics this level cannot be firmly established in the level scheme. Therefore, it is neither shown in Fig. 1 nor included in Table II.

Figure 2(a) shows a spectrum in coincidence with the 622 keV line and either the 246 or 571 keV transitions. It shows a line at 934 keV, which connects the previously known levels at 1439 and 2374 keV. In addition, a weak line is present at 794 keV, which is clearly seen in the inset of Fig. 2(a). By investigating single and double coincidence spectra involving the 794 and 934 keV transitions it is found that these two transitions are not in coincidence with each other. In the spectrum in coincidence with the 794 keV line the 246, 571, and 622 keV transitions all have the same intensity within uncertainties. Consequently, there has to be a new state at 2234 keV. The existence of this level is further supported by the presence of a weak line at 1417 keV, which is evidenced in Fig. 2(d). In this spectrum, which is in double coincidence with the 1417 keV line and either the 246 or

571 keV transition, only the latter two transitions are clearly seen. If the 1417 keV transition were feeding into any other state but the one at 817 keV, there should be a third transition in the spectrum with about twice the statistics of the 246 or 571 keV transition, respectively. In particular, there are at most three (background) counts in Fig. 2(d) at the position of the intense 376 keV  $5^+ \rightarrow 3^+$  transition. The weak 1417 keV branch thus feeds directly into the 817 keV  $3^+$  yrast state.

The spectrum of Fig. 2(c) was taken in coincidence with the 1488 keV transition and any of the three lines at 246, 376, or 571 keV. Clearly, peaks are visible at 867, 946, 1023, and 1241 keV, which confirm the above mentioned bypass of the 2355 keV transition as well as the presence of the 4945 keV level.

Special emphasis was put into the search for candidates for the  $T=1$   $2^+$  level, which can be expected to lie energetically somewhere near the 954 keV  $2^+$  isobaric analog state in  $^{62}\text{Zn}$ . The signature would be low-energy isovector magnetic dipole transitions into the  $T=0$  571 keV  $1^+$  and 817 keV  $3^+$  states, eventually supported by the existence of a stretched quadrupole  $2^+ \rightarrow 0^+$  ground-state decay. Figure 3(a) shows a

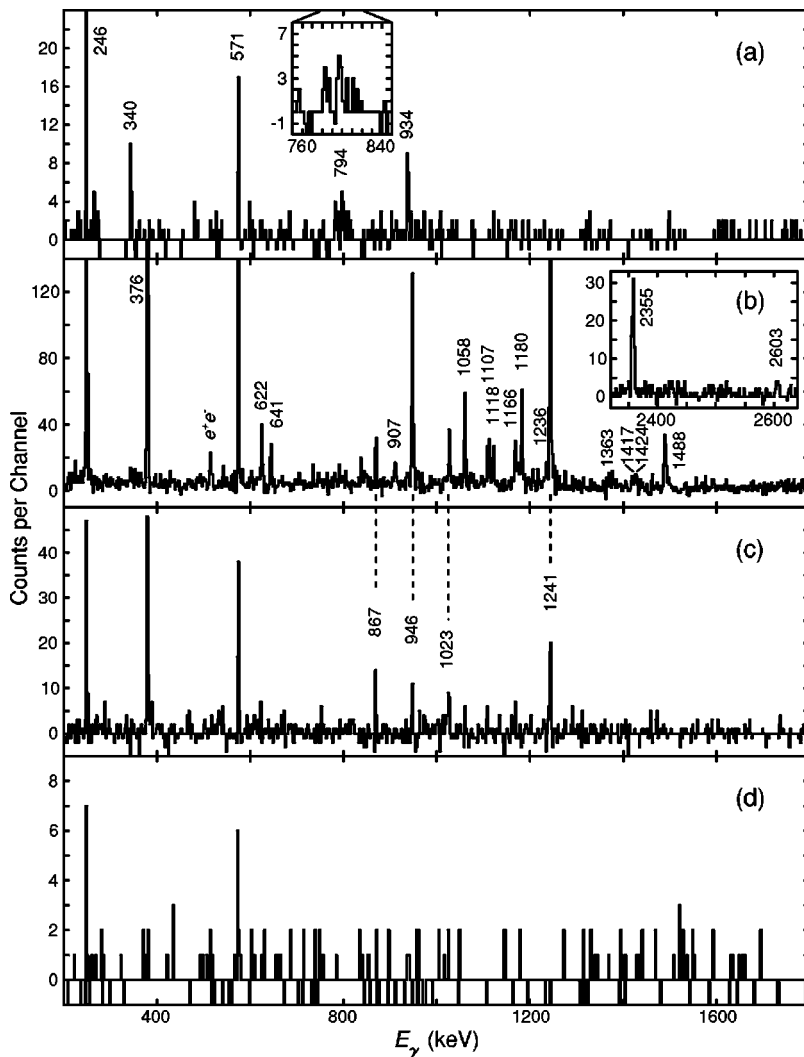


FIG. 2.  $\gamma$ -ray spectra resulting from a  $\gamma\gamma$  analysis. All spectra are gated with zero  $\alpha$  particles and zero or one proton detected in ISIS and any number of neutrons. The peaks are labeled with their energies in keV. Panel (a) is in double coincidence with the 246 or 571 keV transition and the 622 keV ( $5_2^+$ )  $\rightarrow$   $3^+$  line. Panel (b) is in coincidence with any combination of the 246, 376, or 571 keV line. Panel (c) is in double coincidence with the 246, 376, or 571 keV transition and the 1488 keV  $8^+ \rightarrow 7^+$  line. Panel (d) is in double coincidence with the 246 or 571 keV transition and the 1417 keV line feeding the 817 keV  $3^+$  state.

spectrum in coincidence with the 571 keV transition including suitable channel selection (see caption). In the energy regime of interest, lines are obvious at 246, 340, and 376 keV, which are placed in the level scheme of Fig. 1. In addition, weak random coincidences with positron annihilation are present at 511 keV, and also transitions from  $^{34}\text{Cl}$ , which arise from reactions of the  $^{24}\text{Mg}$  beam on the  $^{12}\text{C}$  contamination of the target. Unfortunately, the 571 keV line in  $^{62}\text{Ga}$  turns out to be contaminated by a 572 keV transition in  $^{34}\text{Cl}$  [22]. Nevertheless, a small unknown peak is seen at 446 keV in Fig. 3(a). A careful investigation of spectra, which are in coincidence with transitions populating and depopulating the same levels as the 572 keV transition in  $^{34}\text{Cl}$ , shows that the 446 keV transition does not belong to this contaminating reaction channel. Furthermore, there is no 446 keV–571 keV coincidence in the  $1\alpha 1p 1n$  reaction channel  $^{58}\text{Cu}$ , the ground-state transition of which is 444 keV [23]. This is evidenced via Fig. 3(b). The 571 keV line is absent in the gray spectrum, which requires a coincidence with an  $\alpha$  particle. Neither the 246 nor the 376 keV transitions are visible in the spectrum of Fig. 3(b). Hence, it is concluded that a 446 keV–571 keV coincidence is observed and attributed to  $^{62}\text{Ga}$ , which gives rise to a level at 1017 keV. A search for a 1017 keV line in the  $1p 1n$ -gated

spectrum, however, proved negative, which may be attributed to insufficient statistics in conjunction with too many contaminating reaction channels (see above), which prevent the preparation of a “purified”  $^{62}\text{Ga}$  reference spectrum.

Spin and parity assignments are based on angular distribution ratios, directional correlations of oriented states, yrast arguments, and the assumption that the 571 keV line feeds the ground state of  $^{62}\text{Ga}$ . For the angular distribution and correlation analysis, the Ge detectors at the most forward ( $35^\circ$  with respect to the beam axis) and the most backward ( $145^\circ$ ) angles of the GASP array were grouped together. According to the symmetry of the angular distribution with respect to  $90^\circ$ , they give rise to one group of detectors at an effective angle of  $\bar{\Theta}=35^\circ$ . The angular distribution ratio  $R_{35-90}$  is formed by comparing the efficiency corrected  $\gamma$ -ray yields in these twelve detectors versus the eight detectors situated at  $90^\circ$ . For the angular correlation analysis more statistics is required. Therefore, we combined the Ge detectors at  $72^\circ$ ,  $90^\circ$ , and  $108^\circ$  to form a second group of detectors at an effective angle of  $\bar{\Theta}=81^\circ$ . The DCO ratio is then defined as [24]

$$R_{DCO}(35-81; \gamma_1, \gamma_2) = \frac{I(\gamma_1 \text{ at } 35^\circ; \text{gated with } \gamma_2 \text{ at } 81^\circ)}{I(\gamma_1 \text{ at } 81^\circ; \text{gated with } \gamma_2 \text{ at } 35^\circ)}.$$

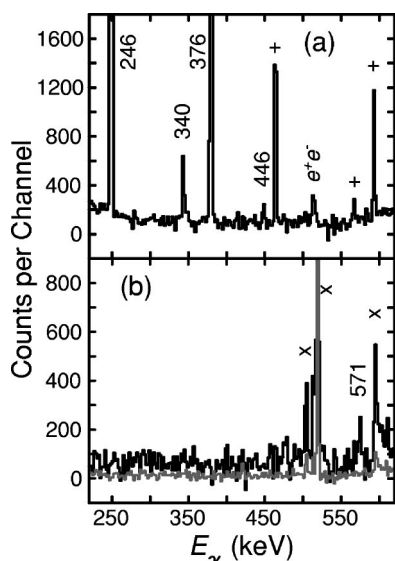


FIG. 3.  $\gamma$ -ray spectra resulting from a  $\gamma\gamma$  analysis. The spectra plotted in black are gated with zero  $\alpha$  particles and zero or one proton detected in ISIS and any number of neutrons. The gray spectrum in panel (b) is in additional coincidence with an  $\alpha$  particle. Panel (a) is in coincidence with the 571 keV ground-state transition of  $^{62}\text{Ga}$ . Peaks labeled with their energies in keV belong to  $^{62}\text{Ga}$ , and peaks labeled with a “+” originate from  $^{34}\text{Cl}$  [22], which are due to reactions on  $^{12}\text{C}$ . Panel (b) is in coincidence with the 446 keV line. The intense peaks in these spectra are from coincidences with the 444 keV ground-state transition in  $^{58}\text{Cu}$ , which is formed via the  $1\alpha 1p 1n$  reaction channel. Note that the 571 keV line is absent in the gray spectrum, and that neither 246 nor the 376 keV transitions are visible.

The DCO ratios were corrected for the different detection efficiencies at different angles. Known intense stretched  $E2$  transitions (246, 376, or 1241 keV) are used for gating. Then one expects  $R_{DCO}=1.0$  for coincident stretched  $E2$  transitions. In principle, DCO ratios of stretched  $\Delta I=1$  or  $\Delta I=0$  transitions depend on the mixing ratio  $\delta(E2/M1)$ . For pure stretched  $\Delta I=1$  transitions  $R_{DCO}\sim 0.6$  is expected for the present geometry.

The experiment does not allow for the distinction between the electric or magnetic character of multipole radiation and, hence, it is, in principle, not possible to determine the parities of the excited states. This uncertainty is accounted for by omitting parity assignments to states, which are found to be only connected to the established part of the level scheme by stretched dipole transitions, i.e., either stretched  $E1$  or stretched  $M1$  radiation.  $E2$  character is always implied for transitions involving quadrupole radiation as no new long-lived isomeric states were observed in the present study, which could hint at an involvement of  $M2$  radiation.

The spin assignments along the odd-spin yrast sequence are straightforward. The  $R_{35-90}$  and  $R_{DCO}$  values call for a pure stretched dipole assignment to the 571 keV transition and for stretched quadrupole character for the 246, 376, 1241, 2355, and 946 keV lines. The yrast character of this sequence manifests itself also in its preferred population with respect to any side structure in the present and previous investigations [14,15].

The nonyrast states require a more careful investigation and more caution when assigning spins and parities. In particular, the possibilities of strongly mixed  $E2/M1$  and  $\Delta I=0$  transitions have to be taken into account. Their DCO values may lie close to unity, similar to the stretched  $E2$  transitions. Yrast arguments can help to distinguish between different options, as well as combinations of several transitions populating and depopulating the state of interest. The newly observed levels are discussed one by one in the following.

The level at 1017 keV is depopulated by the 446 keV transition. Its angular distribution ratio  $R_{35-90}=0.58(9)$  is a clear sign of a stretched dipole transition. Statistics are too low to deduce a DCO ratio for the 446 keV transition. Hence, spin  $I=2$  can be assigned to the 1017 keV level, while its parity remains open.

The level at 1439 keV is depopulated by the relatively intense 622 keV transition and fed by three weak  $\gamma$  rays at 794, 934, and 1236 keV. The angular distribution and correlation measurements of the 622 keV line are consistent with a stretched  $E2$  transition, i.e., with a spin-parity assignment of  $I^\pi=5^+$  to the 1439 keV level. An alternative is a strongly mixed  $\Delta I=1$  transition, i.e.,  $I^\pi=4^+$ , which is supported by the angular distribution value of the 934 keV transition feeding from the 2374 keV level. The option  $I=3$  is excluded due to the connections to the 2374 and 2675 keV levels.

The experimental numbers derived for the state at 2234 keV are associated with relatively large uncertainties. Nevertheless, the value  $R_{35-90}(1417\text{ keV})=0.77(23)$  points towards a spin  $I=4$  assignment. The energetic location also makes it a prime candidate for the  $T=1$ ,  $I^\pi=4^+$  isobaric analog state.

The spin and parity of the 2374 keV level can be fixed to  $I^\pi=6^+$  with the help of the DCO ratio and the angular distribution ratio of the depopulating 1180 keV transition. While the former is consistent with both a stretched  $E2$  and a mixed  $\Delta I=1$ ,  $E2/M1$  transition, the latter excludes an  $E2$  assignment. In addition, if the 1180 keV transition were of  $E2$  character, the 2374 keV state would represent the yrast  $7^+$  state, which is at variance with the intensity pattern of the decay scheme.

The only number available for the 2675 keV level, i.e.,  $R_{35-90}(1481\text{ keV})=0.62(11)$ , fixes its spin to  $I=6$ . The parity cannot be determined.

The state at 3015 keV is populated by the 907 keV transition and depopulated by the 340 and 641 keV transitions. Yrast arguments prevent a spin assignment in excess of  $I=7$ , and the measured ratios for the 641 and 907 keV transitions are consistent with either a  $I^\pi=6^+$  or  $I^\pi=7^+$  assignment. The latter, however, is considered more likely, as the  $R_{35-90}(907\text{ keV})$  value is not fully consistent with an  $E2$  character of that transition.

The 3492 keV level is depopulated by the 1058 and 1118 keV transitions. The latter defines the spin  $I=7$  due to its stretched  $\Delta I=1$  character, and the values for the 1058 keV transition are consistent with the derived  $\Delta I=0$  character. The parity of this state remains unknown.

The level at 3922 keV is connected to both the yrast  $7^+$  and  $9^+$  states via the 1488-867 keV cascade. The DCO ratios for both transitions are relatively low and indicate stretched

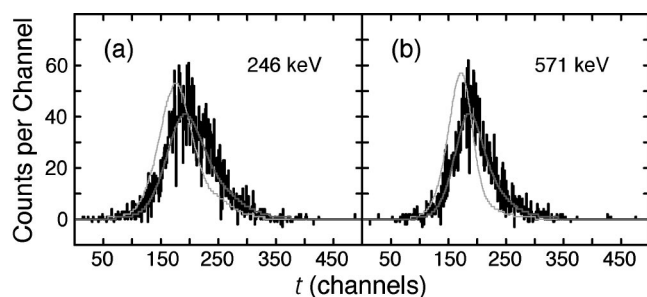


FIG. 4. Time spectra of the 246 (a) and 571 keV (b) transitions, which are situated below the previously known isomeric  $3^+$  state at 817 keV. The spectra are gated with zero  $\alpha$  particles and zero or one proton detected in ISIS, and they are in coincidence with the 376 keV  $5^+ \rightarrow 3^+$  transition. The light gray curves represent the prompt time distributions at the respective  $\gamma$ -ray energy, and the dark gray curves the result of least squares fits to the data.

$\Delta I=1$ , mixed  $E2/M1$  character, i.e., the spin and parity of the 3922 keV state is  $I^\pi=8^+$ .

The two ratios of the 1166 keV transition, which depopulates the 4658 keV level, are seemingly consistent with mixed dipole or stretched  $E2$  character. However, the  $R_{35-90}(1166 \text{ keV})$  value lies on the low side of a possibly stretched  $E2$  character, and yrast arguments clearly favor the  $\Delta I=1$  option, i.e., we assign spin  $I=8$  to the state at 4658 keV.

The situation for the 4945 keV level is similar to the preceding 4658 keV state. The numbers of the depopulating 1023 keV transition are, in principle, consistent with  $I^\pi=9^+$  or  $I^\pi=10^+$  assignments, while the  $I^\pi=9^+$  assignment is more likely due to the relatively small  $R_{35-90}(1023 \text{ keV})$  value and yrast arguments.

In Ref. [14] the 817 keV  $3^+$  state was found to be isomeric with a lifetime of  $\tau=4.6(16)\text{ns}$ . The result was derived by applying the recoil distance decay technique. Figure 4 provides the results of a lifetime analysis using the time spectra of the Ge detectors of GASP. The measured time spectra (black in Fig. 4) of the 246 and 571 keV transitions are overlaid with the measured prompt time spectra at the respective  $\gamma$ -ray energy (light gray curves) and the result of a least squares fitting procedure (dark gray curves). The latter employed the prompt time distribution folded with an exponential decay function. Combining the analysis of the 246 and 571 keV transitions a lifetime for the 817 keV  $3^+$  state of  $\tau=5.8^{(30)}_{(21)} \text{ ns}$  can be derived, which is consistent with the previous number. The weighted average of the two measurements amounts to  $\bar{\tau}=4.9^{(14)}_{(13)} \text{ ns}$  corresponding to a reduced transition strength of  $B(E2; 3^+ \rightarrow 1^+) \sim 180e^2 \text{ fm}^4 \sim 13 \text{ W.u.}$  (W.u., Weisskopf unit).

#### IV. DISCUSSION

The previously known excitation scheme of  $^{62}\text{Ga}$  [14,15] has been subject to several investigations within different theoretical approaches. For example, spherical shell-model calculations [14,25,26] in the  $pf_{5/2}g_{9/2}$  space, deformed shell-model calculations [27], the cranked Nilsson-Strutinsky for-

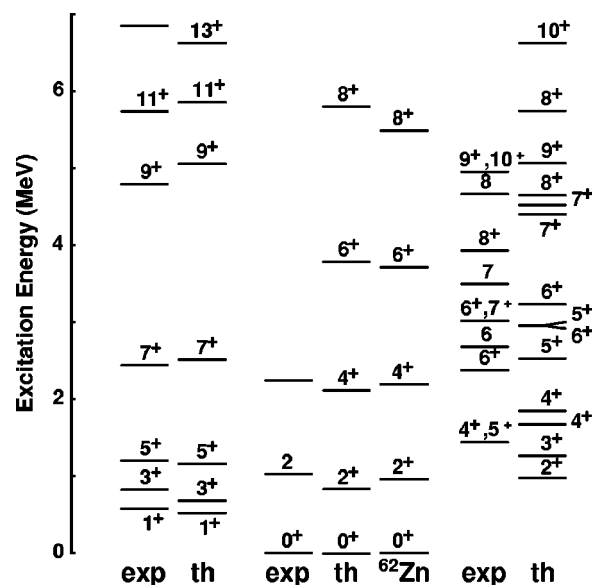


FIG. 5. Comparison of the experimental (exp) and predicted (th) level energies in  $^{62}\text{Ga}$  for the odd-spin  $T=0$  sequence (left), the possible  $T=1$  sequence (middle), and the nonyrast states (right). For completeness, the ground-state band of  $^{62}\text{Zn}$  is included in the middle part. The predicted level energies have been adjusted according to a binding energy shift of  $\text{BES}=-15 \text{ keV}$  derived from the ground state and the odd-spin  $T=0$  states.

malism [26], or the IBM-4 model [25] have been applied. There are two main reasons for the theoretical interest:  $^{62}\text{Ga}$  is an odd-odd  $N=Z$  nucleus and by such it may carry important information on competing  $T=0$  and  $T=1$  excitation modes or, in more general terms, isospin effects. Second, it lies in the vicinity the doubly magic nucleus  $^{56}\text{Ni}$ . On the one hand, the seemingly small number of six valence particles with respect to  $^{56}\text{Ni}$ , three neutrons and three protons, implies that already at medium to high spins the soft  $^{56}\text{Ni}$  core [28] may break. On the other hand,  $1g_{9/2}$  intruder orbitals rapidly approach the Fermi surface once the nucleus drifts to prolate deformation. Consequently, for a complete description of  $^{62}\text{Ga}$  a large model space including the full  $fp$  shell and the  $g_{9/2}$  subshell is probably necessary, while any additional experimental information on  $^{62}\text{Ga}$  can serve to restrict the respective parameter sets. A full  $fp g_{9/2}$  model space calculation is not yet available for  $^{62}\text{Ga}$  with the present-day computational limits. In this paper a spherical shell-model calculation is presented in the  $pf_{5/2}g_{9/2}$  valence space, corresponding to a closed  $^{56}\text{Ni}$  core. We use the effective interaction from Ref. [14], which gave a very good spectroscopy of low-lying yrast states in  $^{62}\text{Ga}$ . The single particle energies from this interaction were borrowed from the  $^{57}\text{Ni}$  spectrum with the  $g_{9/2}$  value taken as 3 MeV. We use now the recently measured value of 3.7 MeV [29] and tuned the monopoles of the interaction to keep the  $^{62}\text{Ga}$  spectrum correct.

The results of the calculations are compared to the experimental data in Fig. 5, which shows the respective level energies. Tables III and IV provide the branchings ratios for the previously known odd-spin  $T=0$  yrast sequence and the new part of the experimental level scheme, respectively. The predicted branching ratios are based on the experimentally ob-

TABLE III. Measured and predicted possible branchings for yrast odd-spin  $T=0$  positive-parity states in  $^{62}\text{Ga}$ . Predicted lifetimes  $\tau_{\text{th}}$  are included for completeness.

$E_x$ (keV)	$\tau_{\text{th}}$ (ps)	$B(E2)_{\text{th}}$ ( $e^2 \text{ fm}^4$ )	$I_i$ ( $\hbar$ )	$I_f$ ( $\hbar$ )	$E_\gamma^a$ (keV)	$b_{\text{exp}}$ (%)	$b_{\text{th}}$ (%)
571	2.9		1 <sub>1</sub>	0 <sub>1</sub>	571	100	100
817	6050	150	3 <sub>1</sub>	1 <sub>1</sub>	246	100	100
1194	510	210	5 <sub>1</sub>	3 <sub>1</sub>	376	100	100
2434	1.4	190	7 <sub>1</sub>	5 <sub>1</sub>	1241	100	100
		1		5 <sub>2</sub>	117		0
				6 <sub>1</sub>	60		0
4789	0.15	76	9 <sub>1</sub>	7 <sub>1</sub>	2355	79(2)	99
		2		7 <sub>2</sub>	1774		1
		1		7 <sub>3</sub>	1297		0
				8 <sub>1</sub>	867	21(2)	0
				8 <sub>2</sub>	131		0
5735	7.9	81	11 <sub>1</sub>	9 <sub>1</sub>	946	94(4)	59
		140		9 <sub>2</sub>	790	6(4)	41
				10 <sub>1</sub>	790		0
6842	2.2	220	13 <sub>1</sub> <sup>b</sup>	11 <sub>1</sub>	1107	100	100

<sup>a</sup>Given as energy differences between the experimental levels. In case these are not known, the energies are estimated using calculated and observed levels.

<sup>b</sup>Taken from Ref. [15].

served level energies, and different options have been probed if the spins of initial and/or final states could not be firmly established. On the left hand side of Fig. 5 the odd-spin  $T=0$  states are shown. Together with the  $0^+$  ground state they give rise to a mean level deviation of 142 keV and a binding energy shift of  $-15$  keV, which is used in Fig. 5 to adjust the calculated level energies. The very good agreement between experiment and theory is striking. The electromagnetic decay properties of this sequence, which are compared in Table III, are also in very good agreement. In addition, the predicted lifetime of the isomeric  $3^+$  state,  $\tau_{\text{th}}=6.05$  ns, matches the experimental value perfectly. It can be noted that the predicted  $B(E2)$  values throughout the odd-spin yrast sequence are equal within a factor of 2, i.e., the isomeric nature of the  $3^+$  state simply arises from the small transition energy.

The only real mismatch in the yrast cascade is found in the decay of the 5735 keV  $11^+$  state. In experiment, the 946 keV branch to the yrast  $9^+$  state is clearly favored, while the calculations predict a split into two almost equally strong transitions into the yrast and yrare  $9^+$  states, the energies of which are almost degenerate in the calculations. It is obvious to associate the 4945 keV level with the yrare  $9^+$  state rather than the yrast  $10^+$  state. The latter is calculated at much too high energy, and the predicted branching would vanish (cf. Table III). Another transition, which is essentially missing in the calculations, is the branch from the yrast  $9^+$  state into the 3922 keV  $8^+$  state. The energy and the decay pattern of the latter are not described very satisfactorily either (see Table IV and below).

The levels at 1439 keV and 2374 keV can be interpreted as the lowest  $4^+$  and  $6^+$   $T=0$  states, respectively. For the 1439 keV level a  $3^+$  assignment would result in a predicted

decay pattern, which is completely wrong (cf. Table IV). The  $5^+$  assignment can be rejected due to the predicted energy of that state, which is more than 1 MeV in excess of the observed energy (cf. Fig. 5). An additional argument in favor of the present  $4^+$  assignment is the 934 keV decay from the 2374 keV state, while the predicted mixing ratio,  $\delta(E2/M1)=-1.5$ , for the 622 keV  $4^+ \rightarrow 3^+$  transition provides a good explanation for its measured  $R_{DCO^-}$  and  $R_{35-90}$  values. Similarly, the 1180 keV  $6^+ \rightarrow 5^+$  transition is predicted to be of almost pure, nonstretched  $E2$  character, which also complies nicely with the experimental angular correlation and angular distribution measurements. While the agreement for the decay pattern of the 2374 keV state is excellent, its predicted energy is about 0.6 MeV too high, which is a mismatch similar to the above mentioned 3922 keV  $8^+$  level. One possible explanation can be the missing  $1f_{7/2}$  one-hole or two-hole excitations, which could be important in this energy and spin regime.

This problem also becomes evident by looking at the new 2675, 3015, 3492, and 4658 keV states. No profound agreement can be inferred between the observed and predicted states and their decays. Energetically, the 2675 keV state is consistent with the predicted  $T=0$   $5^+$  or  $6^+$  levels. In terms of decay pattern, however, one would like to associate this state with the predicted lowest  $6^+$  state, but this is already assigned to the observed level at 2374 keV. The situation becomes worse for the other three states, as the predicted  $7^+$  state is calculated at 4408 keV and the  $8^+$  state at 5755 keV. There are, however, configurations of either parity, which can be expected relatively low in energy, but which are missing in the calculations due to the restrictions in the model space. The  $7^+$  configuration  $[\pi(1f_{7/2})^{-1} \times \nu(1f_{7/2})^{-1}]_7$ , which

TABLE IV. Measured and predicted possible branchings for nonyrast states in  $^{62}\text{Ga}$ . For most of the states, several options are presented corresponding to insecure experimental spin assignments or potential agreement between observed and calculated level energies.

$E_x$ (keV)	$I_{i,\text{exp}}^\pi$ ( $\hbar$ )	$I_{i,\text{th}}$ ( $\hbar$ )	$T_{i,\text{th}}$	$I_f$ ( $\hbar$ )	$E_\gamma^a$ (keV)	$b_{\text{exp}}$ (%)	$b_{\text{th}}$ (%)		
1017	2	$2_1$	1	$0_1$	1017		81		
				$1_1$	446	100	19		
				$3_1$	200		0		
		$2_2$	0	$0_1$	1017		0		
				$1_1$	446	100	87		
				$2_1$	63 <sup>b</sup>		12		
				$3_1$	200		0		
		1439	$4^+, 5^+$	$3_2$	0	$1_1$	868		5
						$2_1$	485 <sup>b</sup>		94
						$2_2$	422		0
$3_1$	622					100	0		
$5_1$	246						0		
$4_1$	0			$2_1$	485 <sup>b</sup>		0		
				$2_2$	422		16		
				$3_1$	622	100	83		
				$3_2$	224		0		
				$5_1$	246		0		
$5_2$	0	$3_1$	622	100	93				
		$3_2$	224		7				
		$5_1$	246		0				
		2234	$4_2$	0	$2_1$	1280 <sup>b</sup>		0	
					$2_2$	1217		11	
$2_3$	823					19			
$3_1$	1417				60(15)	61			
$3_2$	707					0			
$4_3$	1		$4_1$	794	40(15)	2			
			$5_1$	1041		6			
			$2_1$	1280 <sup>b</sup>		31			
			$2_2$	1217		0			
			$2_3$	954		0			
$5_2$	0	$3_1$	1417	60(15)	8				
		$3_2$	839		10				
		$4_1$	794	40(15)	36				
		$4_2$	443		15				
		$5_1$	1041		0				
2374	$6^+$	$5_2$	0	$3_1$	1557		22		
				$3_2$	1120		53		
				$3_1$	1557		22		
				$3_2$	1120		53		

TABLE IV. (*Continued.*)

$E_x$ (keV)	$I_{i,\text{exp}}^\pi$ ( $\hbar$ )	$I_{i,\text{th}}$ ( $\hbar$ )	$T_{i,\text{th}}$	$I_f$ ( $\hbar$ )	$E_\gamma^a$ (keV)	$b_{\text{exp}}$ (%)	$b_{\text{th}}$ (%)
2675	6	$5_2$	0	$3_3$	690		2
				$4_1$	934	23(3)	21
				$4_2$	617		0
				$4_3$	140		1
				$5_1$	1180	77(3)	0
		$6_1$	0	$4_1$	934	23(3)	31
				$4_2$	759		8
				$4_3$	140		0
				$5_1$	1180	77(3)	62
				$5_2$	121		0
3015	$6^+, 7^+$	$6_2$	0	$3_1$	1858		19
				$3_2$	1269		36
				$3_3$	1024		5
				$4_1$	1236	36(20)	29
				$4_2$	873		0
		$5_3$	0	$4_3$	441		10
				$5_1$	1481	64(20)	0
				$6_1$	301		0
				$7_1$	241		0
				$3_1$	1858		53
3015	$6^+, 7^+$	$6_2$	0	$3_2$	1486		0
				$3_3$	1241		20
				$4_1$	1236	36(20)	2
				$4_2$	1090		13
				$4_3$	441		10
		$6_1$	0	$5_1$	1481	64(20)	2
				$5_2$	275		0
				$6_1$	301		0
				$7_1$	241		0
				$4_1$	1236	36(20)	34
3015	$6^+, 7^+$	$6_2$	0	$4_2$	1087		13
				$4_3$	441		0
				$5_1$	1481	64(20)	53
				$5_2$	301		0
				$7_1$	241		0
		$6_2$	0	$4_1$	1236	36(20)	41
				$4_2$	1064		58
				$4_3$	441		0
				$5_1$	1481	64(20)	0
				$5_2$	301		0
3015	$6^+, 7^+$	$6_2$	0	$6_1$	301		0
				$7_1$	241		0
				$4_1$	1576		38
				$4_2$	1397		62
				$4_3$	781		0
3015	$6^+, 7^+$	$6_2$	0	$5_1$	1822		0
				$5_2$	641	54(8)	0

TABLE IV. (Continued.)

$E_x$ (keV)	$I_{i,\text{exp}}^\pi$ ( $\hbar$ )	$I_{i,\text{th}}$ ( $\hbar$ )	$T_{i,\text{th}}$	$I_f$ ( $\hbar$ )	$E_\gamma^a$ (keV)	$b_{\text{exp}}$ (%)	$b_{\text{th}}$ (%)
				6 <sub>1</sub>	340	46(8)	0
				7 <sub>1</sub>	581		0
		7 <sub>2</sub>	0	5 <sub>1</sub>	1822		37
				5 <sub>2</sub>	641		58
				5 <sub>3</sub>	340		1
				6 <sub>1</sub>	641	54(8)	3
				6 <sub>2</sub>	340	46(8)	1
				7 <sub>1</sub>	581		1
3492	7	7 <sub>2</sub>	0	5 <sub>1</sub>	2299		9
				5 <sub>2</sub>	1118		74
				5 <sub>3</sub>	817		5
				6 <sub>1</sub>	1118	32(3)	4
				6 <sub>2</sub>	817		7
				7 <sub>1</sub>	1058	68(3)	2
3922	8 <sup>+</sup>	8 <sub>1</sub>	0	6 <sub>1</sub>	1548		82
				6 <sub>2</sub>	1247		1
				6 <sub>3</sub>	125		0
				7 <sub>1</sub>	1488	69(3)	17
				7 <sub>2</sub>	907	31(3)	0
				7 <sub>3</sub>	430		0
4658	8	8 <sub>2</sub>	0	6 <sub>1</sub>	2284		1
				6 <sub>2</sub>	1983		97
				6 <sub>3</sub>	861		0
				7 <sub>1</sub>	2224		1
				7 <sub>2</sub>	1643		1
				7 <sub>3</sub>	1166	100	0
				8 <sub>1</sub>	736		0
4945	9 <sup>+</sup> , 10 <sup>+</sup>	9 <sub>2</sub>	0	7 <sub>1</sub>	2511		99
				7 <sub>2</sub>	1930		1
				7 <sub>3</sub>	1453		0
				8 <sub>1</sub>	1023	100	0
				8 <sub>2</sub>	287		0
				9 <sub>1</sub>	156		0

<sup>a</sup>Given as energy differences between the experimental levels. In case these are not known, the energies are estimated using calculated and observed levels.

<sup>b</sup>Assuming  $E_x(2_1^+, T=1, ^{62}\text{Ga}) = E_x(2_1^+, T=1, ^{62}\text{Zn}) = 954$  keV.

is significant for the yrast 3420 keV 7<sup>+</sup> state in  $^{58}\text{Cu}$  [6], and 7<sup>-</sup> and 8<sup>-</sup> configurations of the type  $[\pi(1f_{7/2})^{-1} \times \nu(1g_{9/2})]_{7,8}$ . The rather isolated nature of the  $I=7$  3492 and  $I=8$  4658 keV states in the level scheme of  $^{62}\text{Ga}$  (see Fig. 1) are candidates for such negative-parity couplings. In fact, negative-parity states have been observed at comparable excitation energies in the two odd-odd  $N=Z+2$  neighbors  $^{64}\text{Ga}$  [30] and  $^{60}\text{Cu}$  [31,32].

It is apparent from Figs. 1 and 5 that the energies of the two candidates for the  $T=1$  isobaric analog states at 1017 and 2234 keV are very reasonable. However, the branching ratios of both states are inconsistent. Based on these, the

$I=2$  1017 keV state should rather be associated with the lowest  $T=0$  2<sup>+</sup> state (cf. Table IV). However, according to its  $R_{35-90}$  value, the 446 keV transition is a rather pure dipole transition, which is expected for an isovector  $M1$  decay. On the contrary, an isoscalar 2<sup>+</sup>  $\rightarrow$  1<sup>+</sup> decay is predicted to comprise a significant quadrupole admixture, which is not the case for the 446 keV transition. For the 2234 keV level the 5<sub>2</sub><sup>+</sup> possibility can be neglected, but the observed decay pattern fits about equally well the predictions for the  $T=0$  4<sub>2</sub><sup>+</sup> and the  $T=1$  4<sup>+</sup> state. This implies that the two states either do not represent the  $T=1$  states of interest, that these inconsistencies are due to restrictions in the calculations, or that the states have negative parity.

At first sight it is somewhat surprising that no strong isovector  $M1$  transitions are predicted between the even-spin  $T=1$  states and the yrast odd-spin  $T=0$  states. Strong isovector  $M1$  transitions are observed and predicted in the lighter odd-odd  $N=Z$  nuclei in the  $fp$  shell, for example, in  $^{46}\text{V}$  [7,2] and  $^{50}\text{Mn}$  [5,8], and reaching strengths up to  $B(M1; 1^+ \rightarrow 0^+) \sim 4\mu_N^2$  in  $^{54}\text{Co}$  [9]. Typically, these  $M1$  transitions dominate the isoscalar stretched  $\Delta I=2$   $E2$  decays. From the theoretical point of view, this dominance has disappeared for  $^{62}\text{Ga}$ , while the experimental results would call for it, if the 1017 and 2234 keV states were interpreted as the  $T=1$  isobaric analog states. The strong  $M1$  transitions in odd-odd  $N=Z$  nuclei can often be associated with quasideuteron configurations [33], which can be viewed as an inert even-even  $N=Z$  core with one valence proton and one valence neutron occupying the same  $j=l+1/2$  orbital. It is demonstrated in Ref. [33] that the  $M1$  strengths of the quasideuteron states differ significantly from cases where the two valence nucleons occupy a  $j=l-1/2$  orbital. Here, the interference of the orbital and spin parts of the  $M1$  operator may lead to almost vanishing  $M1$  matrix elements.  $^{62}\text{Ga}$  is situated in the upper  $fp$  shell, where the dominant orbitals for the low-spin excitations are  $2p_{3/2}$  ( $j=l+1/2$ ) and  $1f_{5/2}$  ( $j=l-1/2$ ). In the quasideuteron scheme particles in the  $2p_{3/2}$  orbital thus favor strong isovector  $M1$  transitions [ $B(M1; 1^+ \rightarrow 0^+) = 4.3\mu_N^2$  using Eq. (12) in Ref. [33]], while particles in the  $1f_{5/2}$  orbital suppress them [ $B(M1; 1^+ \rightarrow 0^+) = 0.028\mu_N^2$  using Eq. (13) in Ref. [33]].

The predicted values of the present shell-model calculation are  $B(M1; 1^+ \rightarrow 0^+) = 0.11\mu_N^2$ ,  $B(M1; 2^+ \rightarrow 1^+) = 0.038\mu_N^2$  for the isovector  $M1$  transitions, which are close to the numbers of the  $1f_{5/2}$  case of the quasideuteron scheme. Only little additional  $2p_{3/2}$  admixtures into the wave functions of these states may drastically change these  $M1$  strengths, which significantly affect both the lifetime of the 1<sup>+</sup> state and the branching of the 446 keV isovector 2<sup>+</sup>  $\rightarrow$  1<sup>+</sup> transition. To check this, we have artificially lowered the  $p_{3/2}$  single particle energy by 1 MeV to favor  $p_{3/2}$  occupancies. The average occupation number of this orbital is increased from 1.5 to 2.2. This causes a dramatic effect on the 1<sup>+</sup>  $\rightarrow$  0<sup>+</sup> and 2<sup>+</sup>  $\rightarrow$  1<sup>+</sup> transition rates, which are increased by more than an order of magnitude to  $0.74\mu_N^2$  and  $1.5\mu_N^2$ , respectively. This indicates that our effective interaction does not reproduce sufficiently accurately the delicate mixing among the  $p_{3/2}$ ,  $p_{1/2}$ , and  $f_{5/2}$  orbitals, although the energy spectrum and the  $B(E2)$  values appear to be satisfactory. This also indicates

that the relevant degrees of freedom for the description of the low-lying states of  $^{62}\text{Ga}$  should be contained in our valence space. We have also checked that particle-hole excitations involving the  $f_{7/2}$  orbital confirm this statement, as they produce no increase of  $M1$  rates.

If one ignores the above mentioned issues and simply considers the 1017 and 2234 keV levels in  $^{62}\text{Ga}$  as the  $T=1$  isobaric analog states to the 954 keV  $2^+$  and 2186 keV  $4^+$  states in  $^{62}\text{Zn}$ , their Coulomb energy differences,  $\text{CED} = E_x^{T=2,4}(^{62}\text{Ga}) - E_x^{T=2,4}(^{62}\text{Zn})$ , would be positive. This is the normal situation seen for basically all known isobaric analog states of this type in medium-mass nuclei with the exception of  $^{70}\text{Br}$ , where the possible anomaly of negative CED values has been associated with the closely lying proton drip line [12].

## V. SUMMARY

A low- to medium-spin study of the odd-odd  $N=Z$  isotope  $^{62}\text{Ga}$  has been presented using a heavy-ion fusion-evaporation reaction at the Coulomb barrier. The previously known excitation scheme has been confirmed, and significant new information has been added in the excitation energy

range  $E_x \sim 1$  to  $\sim 5$  MeV. It has been possible to present candidates for the  $2^+$  and  $4^+$  isobaric analog states of the  $T_z=1$  neighbor  $^{62}\text{Zn}$ . Clearly, more spectroscopic information is necessary, for example, lifetime measurements, and other reaction types have to be explored. However,  $(p, n\gamma)$  reactions, which have successfully been used for detailed low-spin studies of  $^{46}\text{V}$  [7],  $^{50}\text{Mn}$  [8], or  $^{54}\text{Co}$  [9], are at present limited to  $A=58$ , since  $^{58}\text{Ni}$  is the last stable  $T_z=1$  nucleus.

The restricted model space, namely, the neglect of excitations from the  $1f_{7/2}$  orbit below the shell closure at  $N=Z=28$  due to computational limitations, could be one explanation for the rather poor description of a number of non-yrast states in the spin range  $I=6$  to  $I=8$ . In turn, the description of the yrast odd-spin  $T=0$  sequence is nearly perfect.

## ACKNOWLEDGMENTS

We would like to thank the accelerator crew at LNL for the excellent support and the target makers at LNL for the preparation of the target. This research was supported by the Swedish Research Council and the European Commission under Contract No. HPRI-1999-CT-00083.

- 
- [1] In *Proceedings of Pingst 2000—Selected Topics on  $N = Z$  Nuclei*, Lund, Sweden, 2000, edited by D. Rudolph and M. Hellström (Bloms i Lund AB, Lund, 2000).
- [2] S. M. Lenzi, D. R. Napoli, C. A. Ur, D. Bazzacco, F. Brandolini, J. A. Cameron, E. Caurier, G. de Angelis, M. De Poli, E. Farnea, A. Gadea, S. Hankonen, S. Lunardi, G. Martínez-Pinedo, Zs. Podolyak, A. Poves, C. Rossi Alvarez, J. Sánchez-Solano, and H. Somacal, *Phys. Rev. C* **60**, 021303(R) (1999).
- [3] C. D. O’Leary, M. A. Bentley, S. M. Lenzi, G. Martínez-Pinedo, D. D. Warner, A. M. Bruce, J. A. Cameron, M. P. Carpenter, C. N. Davids, P. Fallon, L. Frankland, W. Gelletly, R. V.F. Janssens, D. T. Joss, C. J. Lister, P. H. Regan, P. Reiter, B. Rubio, D. Seweryniak, C. E. Svensson, S. M. Vincent, and S. J. Williams, *Phys. Lett. B* **525**, 49 (2002).
- [4] A. F. Lisetskiy, A. Schmidt, I. Schneider, C. Friessner, N. Pietralla, and P. von Brentano, *Phys. Rev. Lett.* **89**, 012502 (2002).
- [5] C. E. Svensson, S. M. Lenzi, D. R. Napoli, A. Poves, C. A. Ur, D. Bazzacco, F. Brandolini, J. A. Cameron, G. de Angelis, A. Gadea, D. S. Haslip, S. Lunardi, E. E. Maqueda, G. Martínez-Pinedo, M. A. Nagarajan, C. Rossi Alvarez, A. Vitturi, and J. C. Waddington, *Phys. Rev. C* **58**, R2621 (1998).
- [6] D. Rudolph, C. Baktash, M. J. Brinkman, M. Devlin, H.-Q. Jin, D. R. LaFosse, L. L. Riedinger, D. G. Sarantites, and C.-H. Yu, *Eur. Phys. J. A* **4**, 115 (1999).
- [7] C. Frießner, N. Pietralla, A. Schmidt, I. Schneider, Y. Utsuno, T. Otsuka, and P. von Brentano, *Phys. Rev. C* **60**, 011304(R) (1999).
- [8] A. Schmidt, I. Schneider, C. Frießner, A. F. Lisetskiy, N. Pietralla, T. Sebe, T. Otsuka, and P. von Brentano, *Phys. Rev. C* **62**, 044319 (2000).
- [9] I. Schneider, A. F. Lisetskiy, C. Frießner, R. V. Jolos, N. Pietralla, A. Schmidt, D. Weisshaar, and P. von Brentano, *Phys. Rev. C* **61**, 044312 (2000).
- [10] P. von Brentano, A. F. Lisetskiy, A. Dewald, C. Frießner, A. Schmidt, I. Schneider, and N. Pietralla, *Nucl. Phys.* **A682**, 48c (2001).
- [11] D. Rudolph, C. J. Gross, J. A. Sheikh, D. D. Warner, I. G. Bearden, R. A. Cunningham, D. Foltescu, W. Gelletly, F. Hannachi, A. Harder, T. D. Johnson, A. Jungclaus, M. K. Kabadyski, D. Kast, K. P. Lieb, H. A. Roth, T. Shizuma, J. Simpson, Ö. Skeppstedt, B. J. Varley, and M. Weiszflog, *Phys. Rev. Lett.* **76**, 376 (1996).
- [12] G. de Angelis, T. Martinez, A. Gadea, N. Marginean, E. Farnea, E. Maglione, S. Lenzi, W. Gelletly, C. A. Ur, D. R. Napoli, Th. Kroell, S. Lunardi, B. Rubio, M. Axiotis, D. Bazzacco, A. M. Bizzeti Sona, P. G. Bizzeti, P. Bednarczyk, A. Bracco, F. Brandolini, F. Camera, D. Curien, M. De Poli, O. Dorvaux, J. Eberth, H. Grawe, R. Menegazzo, G. Nardelli, J. Nyberg, P. Pavan, B. Quintana, C. Rossi Alvarez, P. Spolaore, T. Steinhart, I. Stefanescu, O. Thelen, and R. Venturelli, *Eur. Phys. J. A* **12**, 51 (2001).
- [13] D. G. Jenkins, N. S. Kelsall, C. J. Lister, D. P. Balamuth, M. P. Carpenter, T. A. Sienko, S. M. Fischer, R. M. Clark, P. Fallon, A. Görgen, A. O. Macchiavelli, C. E. Svensson, R. Wadsworth, W. Reviol, D. G. Sarantites, G. C. Ball, J. Rikovsky Stone, O. Juillet, P. Van Isacker, A. V. Afanasjev, and S. Frauendorf, *Phys. Rev. C* **65**, 064307 (2002).
- [14] S. M. Vincent, P. H. Regan, D. D. Warner, R. A. Bark, D. Blumenthal, M. P. Carpenter, C. N. Davids, W. Gelletly, R. V.F. Janssens, C. D. O’Leary, C. J. Lister, J. Simpson, D. Seweryniak, T. Saitoh, J. Schwartz, S. Törmänen, O. Juillet, F. Nowacki, and P. Van Isacker, *Phys. Lett. B* **437**, 264 (1998).
- [15] T. Steinhardt, Diploma thesis, University of Cologne, 1997.

- [16] J. Huo and B. Singh, Nucl. Data Sheets **91**, 317 (2000).
- [17] C. Andreoiu, M. Axiotis, G. de Angelis, J. Ekman, C. Fahlander, E. Farnea, A. Gadea, T. Kröll, S. M. Lenzi, N. Mărginean, T. Martinez, M. N. Mineva, C. Rossi Alvarez, D. Rudolph, and C. A. Ur, Eur. Phys. J. A **15**, 459 (2002).
- [18] D. Bazzacco, in *Proceedings of International Conference on Nuclear Structure at High Angular Momentum, Ottawa, Canada, 1992*, edited by D. Ward and J. C. Waddington (AECL Research Report No. AECL 10613), Vol. II, p. 376; C. Rossi Alvarez, Nucl. Phys. News **3**, 3 (1993).
- [19] E. Farnea, G. de Angelis, M. De Poli, D. De Acuña, A. Gadea, D. R. Napoli, P. Spolaore, A. Buscemi, R. Zanon, R. Isocrate, D. Bazzacco, C. Rossi Alvarez, P. Pavan, A. M. Bizzeti-Sona, and P. G. Bizzeti, Nucl. Instrum. Methods Phys. Res. A **400**, 87 (1997).
- [20] D. C. Radford, Nucl. Instrum. Methods Phys. Res. A **361**, 297 (1995).
- [21] J. Theuerkauf, S. Esser, S. Krink, M. Luig, N. Nicolay, O. Stuch, and H. Wolters (unpublished).
- [22] P. M. Endt, Nucl. Phys. **A521**, 1 (1990); **A633**, 1 (1998).
- [23] D. Rudolph, D. G. Sarantites, C. Andreoiu, C. Fahlander, D. P. Balamuth, R. J. Charity, M. Devlin, J. Eberth, A. Galindo-Uribarri, P. A. Hausladen, D. Seweryniak, L. G. Sobotka, and Th. Steinhardt, Eur. Phys. J. A **14**, 137 (2002).
- [24] K. S. Krane, R. M. Steffen, and R. M. Wheeler, At. Data Nucl. Data Tables **11**, 351 (1973).
- [25] O. Juillet, P. Van Isacker, and D. D. Warner, Phys. Rev. C **63**, 054312 (2001).
- [26] A. Juodagalvis and S. Åberg, Nucl. Phys. **A683**, 207 (2001).
- [27] R. Sahu and V. K.B. Kota, Phys. Rev. C **66**, 024301 (2002).
- [28] T. Otsuka, M. Honma, and T. Mizusaki, Phys. Rev. Lett. **81**, 1588 (1998).
- [29] D. Rudolph, D. Weisshaar, F. Cristancho, J. Eberth, C. Fahlander, O. Iordanov, S. Skoda, Ch. Teich, O. Thelen, and H. G. Thomas, Eur. Phys. J. A **6**, 377 (1999).
- [30] B. Singh, Nucl. Data Sheets **78**, 395 (1996).
- [31] Tsan Ung Chan, M. Agard, J. F. Bruandet, B. Chambon, A. Dauchy, D. Drain, A. Giorni, F. Glasser, and C. Morand, Phys. Rev. C **26**, 424 (1982).
- [32] O. Izotova, Master thesis, Lund University, 2003.
- [33] A. F. Lisetskiy, R. V. Jolos, N. Pietralla, and P. von Brentano, Phys. Rev. C **60**, 064310 (1999).